

# Stability analysis of digitally controlled dual active bridge converters

Ling SHI<sup>1</sup>, Wanjun LEI<sup>1</sup> , Zhuoqiang LI<sup>1</sup>, Yao CUI<sup>1</sup>, Jun HUANG<sup>1</sup>, Yue WANG<sup>1</sup>



**Abstract** The dual active bridge (DAB) converters are widely used in the energy storage equipment and the distributed power systems. However, the existence of switching nonlinearity and control delay can cause serious stability problem to the DAB converters. Thus, this paper, studies the stability of a digitally controlled DAB converter with an output voltage closed loop controller. Firstly, to accurately study the stability in a DAB converter, a discrete-time model established in a whole switching period is obtained. The model considers the output capacitor ESR, the digital control delay, and sample-and-hold process. By using this model, the stabilities of the DAB converter versus the proportional controller parameter and the output capacitor ESR are analyzed and the critical values are predicted accurately. Moreover, the stability boundary of

the proportional controller parameter and the output capacitor ESR is also obtained. The result shows that the value of the output capacitor ESR can have a great effect on the stability region of the proportional controller parameter. Finally, the theoretical analyses are verified by the simulation and experimental results.

**Keywords** Dual active bridge (DAB), Discrete time modeling, Stability analysis, Dynamics

## 1 Introduction

Applications such as plug-in hybrid electric vehicles [1], renewable energy storage [2], uninterruptible power supply (UPS) systems [3], aerospace applications [4] and smart grids [5] usually need an energy storage device, which increase the popularity of the bidirectional DC-DC converters. As the DAB converter has many advantages, such as galvanic isolation, zero-voltage switching, high power density, high efficiency, and symmetric structure [6], it has been drawn more attention compared with other bidirectional DC-DC converters. Until now, researchers have focused on modeling [7], control strategies [8–10], design methodology [11], and modulation strategies [3, 12]. However, the complex dynamics in the digitally controlled DAB converter, caused by switching nonlinearity and control delay [13], may deteriorate the working performance and bring stability problem. However, it has not been studied in the existing literature.

Because of the inherent nonlinearity existing in DC-DC converters, the systems may always show the abnormal operation instead of the expected normal operation. To study dynamic behavior and stability of the DC-DC converters, many researchers have devoted to the modeling

CrossCheck date: 14 June 2017

Received: 27 April 2016 / Accepted: 15 June 2017 / Published online: 30 August 2017

© The Author(s) 2017. This article is an open access publication

✉ Wanjun LEI  
leiwanjun@xjtu.edu.cn

Ling SHI  
xdshiling0821@163.com

Zhuoqiang LI  
lizhuoqiang20@stu.xjtu.edu.cn

Yao CUI  
cuiyao1618@stu.xjtu.edu.cn

Jun HUANG  
hjxjtu@stu.xjtu.edu.cn

Yue WANG  
davidwangyue@xjtu.edu.cn

<sup>1</sup> State Key Laboratory of Electrical Insulation and Power Equipment, Shaanxi Key Laboratory of Smart Grid, Xi'an Jiaotong University, Xi'an 710000, China



methods, and various kinds of complex dynamics have been investigated, such as Hopf bifurcation, period doubling bifurcation and chaos [14–16]. Generally, a state-space averaged model or a discrete-time model can be used to study the dynamics in converters [17, 18]. The averaged model averages each circuit variable within one switching period. Thus, this model neglects the switching details and can only detect the slow-scale dynamics of the system effectively. The discrete-time model expresses the state variables at one sampling time and the variables at an earlier sampling time by deriving an iterative function. This model can offer information of both the slow-scale and fast-scale dynamics of the system and is more accurate compared with the averaged model.

To study the dynamics in a DAB converter, an appropriate model should be developed first. Considering the small ripple requirement in averaged model [17], establishing a discrete-time model is more appropriate as the transformer current in a DAB converter is purely AC. Thus, several discrete-time models for DAB converters have been established. In [19], a discrete-time averaged model is obtained. This model averages the value of the output voltage over half switching period and suitable for half period control. In [20, 21], due to the symmetry of the transformer current and the output voltage in steady state, the discrete-time models are also established in a half switching period and suitable for half period control. In [22], a discrete-time small signal model is developed. It is established in a full switching period. However, it does not consider the ESRs in circuit. Above of all, almost all of these models have not consider the output capacitor ESR. But when one switching period control is adopted and the system loses stability under inappropriate parameters, the state variables will be unsymmetrical. The previous models suitable for half switching period control will not be suitable anymore and a more accurate model should be established. Thus, in this paper, a full discrete-time model in a whole switching period is established. This model considers all the ESRs in the circuit, including the output capacitor ESR. Using this model, the influences of the controller parameter and the output capacitor ESR on the stability of the system are discussed. Simulation and experimental results show that this full discrete-time model is effective enough and can predict the instability of the system accurately.

The rest of the paper is organized as follows. The operation principle of the digitally controlled DAB converter is briefly introduced and the full discrete-time model is established in Section 2. Then, in Section 3, based on the full discrete-time model, the stability of the DAB converter is analyzed. In Section 4, simulation and experimental results verify the theoretical analyses. Finally, conclusions are given in Section 5.

## 2 System description and full discrete-time modeling

### 2.1 System description

The schematic circuit of a digitally controlled DAB converter is shown in Fig. 1. It consists of a power stage and a digital control system. The power stage is composed mainly of a high frequency transformer and two H bridges.

The turn ratios of high-frequency transformer is  $1:N$ . The transformer provides voltage matching and galvanic isolation between two voltage buses. Owing to the symmetrical structure, DAB converter can realize bidirectional power flow. In this paper, take the power flowing from  $V_1$  to  $V_2$  as an example. So  $V_1$  is the input DC voltage,  $V_2$  is the output voltage.  $L$  is the transformer leakage inductance, serving as an instantaneous energy storage device.  $R_t$  is the sum of the line resistances, the switch on-resistors, and the transformer winding resistances.  $C_o$  is the output capacitor.  $R_C$  is the output capacitor ESR.

Generally, a DAB converter has four control strategies [6]. They are respectively the single phase-shift (SPS) control, the extended-phase-shift (EPS) control, the dual-phase-shift (DPS) control, and the triple-phase-shift (TPS) control. The SPS control, which is the most widely used control strategy for DAB converters [1, 6, 23], is adopted in this paper. In SPS control,  $v_p$  and  $v_s$  are square wave voltages with 50% duty cycle. The phase shift  $\varphi$  between  $v_p$  and  $v_s$  controls the power flow directions. Figure 2 is the operation waveforms in steady state and in this case, the power flows from the  $V_1$ -side to the  $V_2$ -side. It can be seen from Fig. 2 that there are four intervals in one switching period and the converter operates symmetrically in each half period.

In this system, the digital controller consists of an output-voltage feedback. It samples the output voltage  $V_2$  at the beginning of each switching period and the sampling

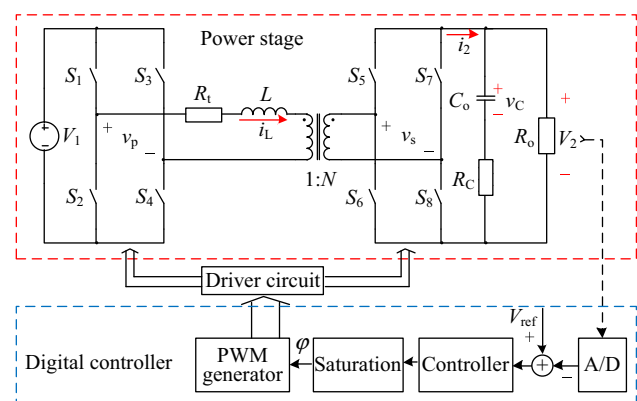
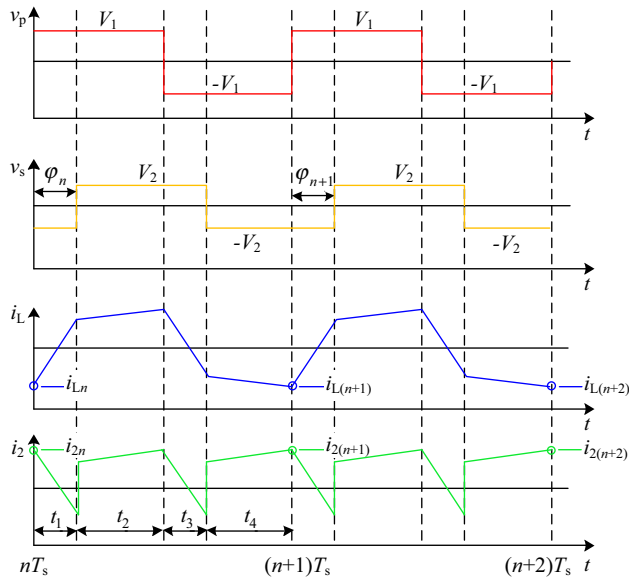


Fig. 1 Diagram of digitally controlled DAB converter



**Fig. 2** Operation waveforms in steady state

result is compared with the voltage reference. Then, the phase shift  $\varphi$  is calculated through the controller and saturator, and loaded at the beginning of the next switching period. Thus, there is one step delay in the system. The saturator element limits the range of  $\varphi$ . When the power flows from  $V_1$  to  $V_2$ , the range of  $\varphi$  is from 0 to  $\pi/2$ . When the power flows from  $V_2$  to  $V_1$ , the range of  $\varphi$  is from  $-\pi/2$  to 0.

The values of the parameters in circuit can have great effect to the stability of the system. An inappropriate parameter can make the phase shift angle  $\varphi$  keep oscillating. Thus, obvious oscillation phenomenon can also appear to the output voltage and the inductor current, making the system in an unstable state. So establishing an appropriate model and using the model to study the stability of the DAB converter is necessary.

## 2.2 Full discrete-time modeling

The discrete-time model derived in this paper assumes that transistor switching transients are negligible. It is also assumed that the input capacitance is relatively large, so the dynamics of the input capacitor are not considered. To obtain the discrete-time model of the converter, continuous time state-space equations of DAB converter in four subintervals should be derived first, each equations taking the form as

$$\dot{\mathbf{x}}(t) = \mathbf{A}_i \mathbf{x}(t) + \mathbf{B}_i V_i \quad (1)$$

where  $\mathbf{x}(t)$  is the state vector and  $\mathbf{x}(t) = [i_L \ v_C]^T$ ;  $i = 1, 2, 3, 4$ , is corresponding to the four subintervals  $t_1$ - $t_4$  in Fig. 2.

The matrices  $\mathbf{A}_i$  and vectors  $\mathbf{B}_i$  in (1) are expressed in (2) and (3). It can be seen from the expressions that this paper considers the output capacitor ESR.

$$\left\{ \begin{array}{l} \mathbf{A}_1 = \mathbf{A}_4 = \begin{bmatrix} -\frac{N^2 R_t + k_1}{N^2 L} & \frac{k_2}{vL} \\ -\frac{k_2}{NC_o} & -\frac{1}{C_o(R_o + R_C)} \end{bmatrix} \\ \mathbf{A}_2 = \mathbf{A}_3 = \begin{bmatrix} -\frac{N^2 R_t + k_1}{N^2 L} & -\frac{k_2}{NL} \\ \frac{k_2}{NC_o} & -\frac{1}{C_o(R_o + R_C)} \end{bmatrix} \end{array} \right. \quad (2)$$

$$\left\{ \begin{array}{l} \mathbf{B}_1 = \mathbf{B}_2 = \begin{bmatrix} \frac{1}{L} & 0 \end{bmatrix} \\ \mathbf{B}_3 = \mathbf{B}_4 = \begin{bmatrix} -\frac{1}{L} & 0 \end{bmatrix} \end{array} \right. \quad (3)$$

where

$$\left\{ \begin{array}{l} k_1 = R_o R_C / (R_o + R_C) \\ k_2 = R_o / (R_o + R_C) \end{array} \right. \quad (4)$$

The discrete-time model is derived from regular sampling of the state variables of the continuous-time dynamics. Compared with the average model, the discrete-time model is obtained without making quasi-static approximation such as high switching frequency and small ripple. The discrete-time modeling process of this system can be divided into two steps. The first step is the power stage and the second step is the digital control system. As the power converter has four switching states in one switching cycle, four discrete-time models in four switching states can be derived by the state variables first, as shown in (5).

$$\left\{ \begin{array}{l} \mathbf{x}(nT_s + t_1) = e^{\mathbf{A}_1 t_1} \cdot \mathbf{x}(nT_s) + \boldsymbol{\psi}_1 V_1 \\ \mathbf{x}(nT_s + t_1 + t_2) = e^{\mathbf{A}_2 t_2} \cdot \mathbf{x}(nT_s + t_1) + \boldsymbol{\psi}_2 V_1 \\ \mathbf{x}(nT_s + t_1 + t_2 + t_3) = e^{\mathbf{A}_3 t_3} \cdot \mathbf{x}(nT_s + t_1 + t_2) + \boldsymbol{\psi}_3 V_1 \\ \mathbf{x}((n+1)T_s) = e^{\mathbf{A}_4 t_4} \cdot \mathbf{x}(nT_s + t_1 + t_2 + t_3) + \boldsymbol{\psi}_4 V_1 \end{array} \right. \quad (5)$$

where

$$\left\{ \begin{array}{l} t_1 = t_3 = \varphi_n / (2\pi f_s) \\ t_2 = t_4 = 1 / (2f_s) - \varphi_n / (2\pi f_s) \end{array} \right. \quad (6)$$

$$\left\{ \begin{array}{l} \boldsymbol{\psi}_1 = \int_0^{t_1} e^{\mathbf{A}_1 t} \mathbf{B}_1 dt = \mathbf{A}_1^{-1} (e^{\mathbf{A}_1 t_1} - \mathbf{I}) \mathbf{B}_1 V_1 \\ \boldsymbol{\psi}_2 = \int_0^{t_2} e^{\mathbf{A}_2 t} \mathbf{B}_2 dt = \mathbf{A}_2^{-1} (e^{\mathbf{A}_2 t_2} - \mathbf{I}) \mathbf{B}_2 V_1 \\ \boldsymbol{\psi}_3 = \int_0^{t_3} e^{\mathbf{A}_3 t} \mathbf{B}_3 dt = \mathbf{A}_3^{-1} (e^{\mathbf{A}_3 t_3} - \mathbf{I}) \mathbf{B}_3 V_1 \\ \boldsymbol{\psi}_4 = \int_0^{t_4} e^{\mathbf{A}_4 t} \mathbf{B}_4 dt = \mathbf{A}_4^{-1} (e^{\mathbf{A}_4 t_4} - \mathbf{I}) \mathbf{B}_4 V_1 \end{array} \right. \quad (7)$$

The discrete-time model in a whole switching cycle can be derived by integrating the four equations in (5). Let the values of  $\mathbf{x}$  at the beginning of the  $n$ -th and the  $(n+1)$ -th

switching cycles be denoted as  $\mathbf{x}_n$ , and  $\mathbf{x}_{n+1}$  respectively, so the discrete-time model of the power stage is shown in (8):

$$\begin{aligned} \mathbf{x}_{n+1} &= e^{A_4 t_4} \{ e^{A_3 t_3} [ e^{A_2 t_2} ( e^{A_1 t_1} \mathbf{x}_n + \boldsymbol{\psi}_1 V_1 ) + \boldsymbol{\psi}_2 V_1 ] \\ &\quad + \boldsymbol{\psi}_3 V_1 \} + \boldsymbol{\psi}_4 V_1 \\ &= \mathbf{F}(\varphi_n) \mathbf{x}_n + \mathbf{G}(\varphi_n) V_1 \end{aligned} \tag{8}$$

where

$$\begin{cases} \mathbf{F}(\varphi_n) = e^{A_4 t_4} \cdot e^{A_3 t_3} \cdot e^{A_2 t_2} \cdot e^{A_1 t_1} \\ \mathbf{G}(\varphi_n) = e^{A_4 t_4} \cdot e^{A_3 t_3} \cdot e^{A_2 t_2} \cdot \boldsymbol{\psi}_1 + e^{A_4 t_4} \cdot e^{A_3 t_3} \cdot \boldsymbol{\psi}_2 \\ \quad + e^{A_4 t_4} \cdot \boldsymbol{\psi}_3 + \boldsymbol{\psi}_4 \end{cases} \tag{9}$$

To simplified calculation and guarantee the accuracy, matrix exponentials involved in (8) can be approximated by the 2-order approximations, as shown in (10)

$$e^{A_m t_m} \approx \mathbf{I} + \mathbf{A}_m t_m + \frac{1}{2!} (\mathbf{A}_m t_m)^2 \tag{10}$$

where  $\mathbf{I}$  is the unit matrix;  $m = 1, 2, 3, 4$ .

The controller system considers one step delay, as it samples  $V_2$  periodically at the time  $t = nT_s$  and updates  $\varphi$  at the time  $t = (n + 1)T_s$ . PI-controller or higher performance controller are frequently used in the DAB system. However, our focus in this paper are the characteristics of the DAB converter instead of the controller. Thus, for simplicity, taking a proportional controller as an example, the discrete-time model of the digital control system is derives as (11), where  $k$  is the proportional controller parameter. It can be observed from the equation that this model deals with one step delay commendably.

$$\varphi_{n+1} = k(V_{\text{ref}} - V_{2n}) = k(V_{\text{refn}} - \mathbf{M} \cdot \mathbf{x}_n) \in [0, \pi/2] \tag{11}$$

where  $V_{\text{refn}}$  is the sampling value at the beginnings of the  $n$ -th switching cycle of the reference voltage  $V_{\text{ref}}$ ; vector  $\mathbf{M}$  describe the relationship among  $V_{2n}$ ,  $i_{L,n}$  and  $v_{Cn}$ .

According to the circuit of  $V_2$  side, the relationship among  $V_2$ ,  $i_2$  and  $v_C$  can be figured out firstly.  $i_2$  is the output current as shown in Fig. 1.

From Fig. 1, it can be easily figured out that

$$V_2 = \frac{R_o R_C}{R_o + R_C} i_2 + \frac{R_o}{R_o + R_C} v_C \tag{12}$$

In the digital controlled DAB converter, it samples the output voltage  $V_2$  periodically at the time  $t = nT_s$ , so the discrete-time equation of (12) is as follows.

$$V_{2n} = \frac{R_o R_C}{R_o + R_C} i_{2n} + \frac{R_o}{R_o + R_C} v_{Cn} \tag{13}$$

The waveform of the inductor current  $i_L$  and the output current  $i_2$  are shown in Fig. 2. The relationship between  $i_L$  and  $i_2$  can be described in (14).

$$\begin{cases} i_2 = i_L/N & t \in [nT_s + t_1, nT_s + t_1 + t_2] \\ i_2 = -i_L/N & t \in [nT_s, nT_s + t_1] \cup [nT_s + t_1 + t_2, (n + 1)T_s] \end{cases} \tag{14}$$

Thus, at the beginning of the  $n$ -th switching cycle, the relationship between  $i_{2n}$  and  $i_{L,n}$  can be described as (15).

$$i_{2n} = -i_{L,n}/N \tag{15}$$

Finally, combined (13) and (15), the vector  $\mathbf{M}$  is obtained as

$$\mathbf{M} = \begin{bmatrix} \frac{-R_o R_C}{(R_o + R_C)N} & \frac{R_o}{R_o + R_C} \end{bmatrix} \tag{16}$$

Above of all, (8) and (11) composes of the full discrete-time model of the digitally controlled DAB converter. Since few mathematical approximations are involved in this model, this model can be considered highly accurate and can be effectively used to predict the dynamics with the variation of parameters in the system.

### 3 Stability analysis of DAB converter

#### 3.1 Jacobian matrix analysis

The parameters in circuit have great influences on the stability of the system. The inductor current and the output voltage waveforms may appear obvious oscillations if the parameters are not well selected. Thus, in this section, the dynamics and stability will be investigated with the help of the Jacobian matrix.

$$\mathbf{J} = \begin{bmatrix} \frac{\partial i_{L(n+1)}}{\partial i_{L,n}} & \frac{\partial i_{L(n+1)}}{\partial v_{Cn}} & \frac{\partial i_{L(n+1)}}{\partial \varphi_n} \\ \frac{\partial v_{C(n+1)}}{\partial i_{L,n}} & \frac{\partial v_{C(n+1)}}{\partial v_{Cn}} & \frac{\partial v_{C(n+1)}}{\partial \varphi_n} \\ \frac{\partial \varphi_{(n+1)}}{\partial i_{L,n}} & \frac{\partial \varphi_{(n+1)}}{\partial v_{Cn}} & \frac{\partial \varphi_{(n+1)}}{\partial \varphi_n} \end{bmatrix}_{(i_L, v_C, \Phi)} \tag{17}$$

Using (8) and (11), the corresponding Jacobian matrix of the system can be expressed as (17). Then the characteristic equation of (17) is shown in (18).

$$\det(\lambda \mathbf{I} - \mathbf{J}) = 0 \tag{18}$$

From (18), we can get all the eigenvalues  $\lambda_{J1}$ ,  $\lambda_{J2}$ , and  $\lambda_{J2}$  of the Jacobian matrix. If at least one eigenvalue exhibits an absolute value higher than 1, then the system is unstable. If the eigenvalues move out of the unit circle from (1, 0) or (-1, 0), saddle node bifurcation or period doubling bifurcation will occur. And conjugated eigenvalues of a discrete-time model crossing out of the unite circle indicates Hopf bifurcation (or Neimarck-Sacker bifurcation) [18].

It should be mentioned that the operation point  $(i_L, v_C, \Phi)$  need to be figured out at the same time to obtain the Jacobian matrix and the eigenvalues. Usually this operating point is in a steady-state and therefore the steady-state solution needs to be calculated. Obviously, the steady-state solution corresponds to constant phase shift angle  $\Phi$

and state vector  $\mathbf{X} = [I_L \ V_C]^T$ . Denote the subintervals  $t_1-t_4$  and exponential matrices in (7) using capitals to represent the steady-state values as in (19).

$$\begin{cases} T_1 = T_3 = \Phi/(2f_s\pi) \\ T_2 = T_4 = 1/(2f_s) - \Phi/(2f_s\pi) \\ \psi_1 = \mathbf{A}_1^{-1}(e^{A_1T_1} - \mathbf{I})\mathbf{B}_1V_1 \\ \psi_2 = \mathbf{A}_2^{-1}(e^{A_2T_2} - \mathbf{I})\mathbf{B}_2V_1 \\ \psi_3 = \mathbf{A}_3^{-1}(e^{A_3T_3} - \mathbf{I})\mathbf{B}_3V_1 \\ \psi_4 = \mathbf{A}_4^{-1}(e^{A_4T_4} - \mathbf{I})\mathbf{B}_4V_1 \end{cases} \quad (19)$$

where  $e^{A_iT_i} = \mathbf{I} + A_iT_i + 0.5(A_iT_i)^2$ ;  $i = 1, 2, 3, 4$ . Then the solution for the operating point  $(I_L, V_C, \Phi)$  can be obtained by enforcing the periodicity:  $\mathbf{x}_{n+1} = \mathbf{x}_n = \mathbf{X}$  in (8), which is given by (20) and (21).

$$\mathbf{X} = (\mathbf{I} - \mathbf{F}(\Phi))^{-1}\mathbf{G}(\Phi)V_1 \quad (20)$$

$$\Phi = k(V_{\text{ref}} - \mathbf{M}\mathbf{X}) \quad (21)$$

The system parameters are shown in Table 1. As we know, all switches in DAB converter can achieve ZVS in whole load range when  $d$  is equal to 1 ( $d$  represents the voltage conversion ratio and  $d=Nv_1/V_2$ ) [24]. So in actually applications, it is optimal to let  $d = 1$ . Thus, in this paper, we use a  $N = 1$  transformer while  $V_1 = V_2$ . If we want to change the parameters of the DAB converter, such as the transformer ratio or input and output voltage, we just change the corresponding parameters in (2) and (5), and the following method in the paper can be directly used.

Based on the parameters above, the effect of the changes of  $k$  will be first investigated. The changing trend and the values of eigenvalues around the border of the unit circle with the increase of  $k$  can be respectively seen in Fig. 3a and Table 2. It can be remarked that there are three eigenvalues, and it is the conjugate eigenvalues exceed the unit circle when  $k$  increases while the third one remains practically unchanged. Therefore, when  $k$  is larger than 0.55, the system is unstable and exhibits Hopf bifurcation.

Then, the output capacitor ESR  $R_C$  is taken as a bifurcation parameter to further illustrate that the choices of parameters have great effect on the stability of the system. Keep  $k$  equal to 0.47 and let  $R_C$  sweep from 0.46  $\Omega$  to 0.7  $\Omega$  with steps of 0.02  $\Omega$ . The trajectory and the values of eigenvalues around the unit circle are respectively shown

**Table 1** System parameters

Parameters	Value	Parameters	Value
$V_1$	30 V	$R_o$	12.5 $\Omega$
$L$	35.49 $\mu\text{H}$	$f_s$	20 kHz
$R_t$	0.38 $\Omega$	$N$	1
$C$	455 $\mu\text{F}$	$V_{\text{ref}}$	30 V
$R_C$	0.45 $\Omega$	$k$	0.1–8

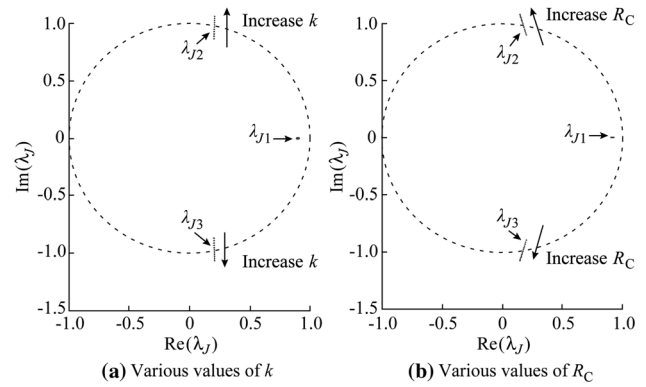


**Fig. 3** Trajectory of eigenvalues

**Table 2** Eigenvalues at  $R_C = 0.45 \Omega$  for various of  $k$

$k$	Eigenvalues $\lambda_{J1}-\lambda_{J3}$	Remarks
0.53	0.8975, $0.2047 \pm 0.9519$	Stable
0.55	0.8964, $0.2052 \pm 0.9715$	Stable
0.57	0.8953, $0.2058 \pm 0.9908$	Unstable
0.59	0.8943, $0.2063 \pm 1.0100$	Unstable

**Table 3** Eigenvalues at  $k = 0.47$  for various of  $R_C$

$R_C(\Omega)$	Eigenvalues $\lambda_{J1}-\lambda_{J3}$	Remarks
0.54	0.9117, $0.1798 \pm 0.9657$	Stable
0.56	0.9137, $0.1753 \pm 0.9812$	Stable
0.58	0.9155, $0.1708 \pm 0.9962$	Unstable
0.60	0.9173, $0.1665 \pm 1.0107$	Unstable

in Fig. 3b and Table 3. It can be remarked that there are also three eigenvalues, and it is the conjugate ones exceed the unit circle when  $R_C$  increases while the third one remains practically unchanged. Thus, when  $R_C$  is bigger than 0.56  $\Omega$ , the system is unstable and exhibits Hopf bifurcation.

### 3.2 Margin of stability curve

In the industry, bifurcations are usually unexpected and avoided and the usual acceptable operation state is period-1 steady state. For example, a Hopf bifurcation can make the system operate at a several periods limit cycle and bring much wider amplitude to the output voltage and inductor current. The wider amplitudes will have greater impact on device stresses. Therefore it is necessary to draw a bifurcation boundary for practical design to avoid the occurrence of such undesirable bifurcations.



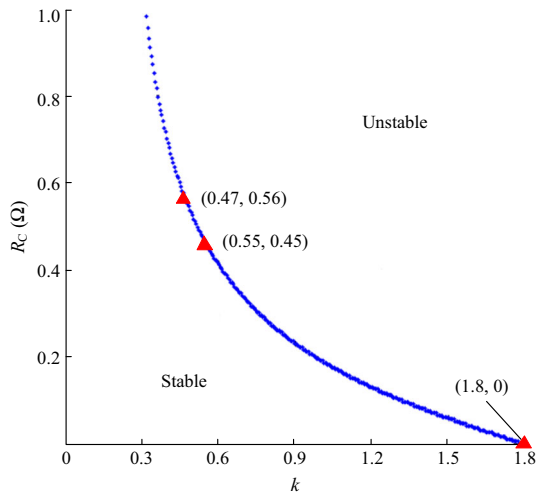


Fig. 4 Stability boundary

The stability boundary at different values of  $k$  and  $R_C$  is demonstrated in Fig. 4. It shows that the stability boundary of  $k$  can be expanded greatly when  $R_C$  is decreased. Thus,  $R_C$  has great influences on the system, which points out that it is quite necessary and important to take  $R_C$  into account in practice. However, it does not mean the system is always stable if  $R_C = 0 \Omega$ . From Fig. 4, it can be seen that when  $R_C = 0 \Omega$ , the system will be unstable when  $k$  is greater than 1.81.

### 4 Simulation results and experimental verifications

In this section, corresponding simulation and experimental studies were conducted to verify the forementioned analysis.

#### 4.1 Simulation results

Based on Fig. 1, the model of a digitally controlled DAB converter is set up in MATLAB/Simulink. In order to simulate the time delay and the sampling and holding process, the “sample time” settings in the unit-delay and sum module are all set as  $T_s$ .

Figure 5 illustrates simulation waveforms of inductor currents with  $0.45 \Omega$  output capacitor ESR when  $k = 0.55$  and  $0.57$ . It can be seen that the digitally controlled system is stable when  $k = 0.55$  and unstable when  $k = 0.57$ , which is coincident with the analysis result of Fig. 3.

When  $R_C = 0.58 \Omega$ , the simulation waveforms when  $k = 0.45$  and  $0.47$  are depicted in Fig. 6. It can be observed that the system is stable when  $k = 0.45$  and unstable when  $k = 0.47$ . Comparing the simulation results of Figs. 5 and 6, it can be found that the increase of  $R_C$  make the stability

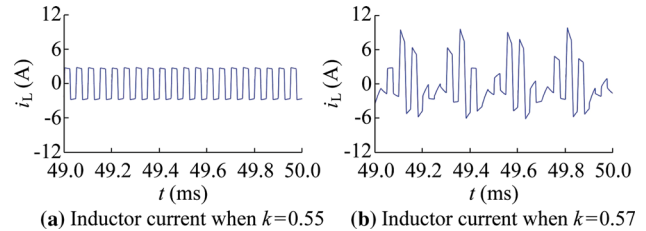


Fig. 5 Simulation results ( $R_C = 0.45 \Omega$ )

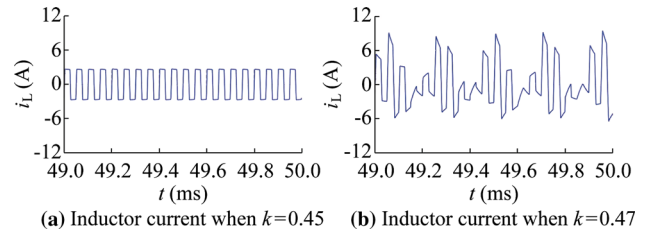


Fig. 6 Simulation results ( $R_C = 0.58 \Omega$ )

boundary of  $k$  decreased, which is consistent with the analysis result of Fig. 4.

#### 4.2 Experimental verifications

For the practical verification, a small-scale experimental prototype was built in the laboratory. It has the same design parameter values with the simulation model to validate the numerical analysis and simulation results.

The functional diagram of the experimental prototype is shown in Fig. 7. The prototype uses “IXFK102N30P” Power MOSFETs from IXYS Corporation as all switches. The external inductor and the transformer are made of litz wires and five electrolytic capacitors are applied as the output capacitor. The converter is controlled with a TMS320F28335 DSP chip, which implements the voltage control algorithm. The output voltage is measured by a LEM Hall voltage sensor and modulated by an output voltage modulating circuit. The 1ED020I12-F driver ICs are applied in the driver circuits to realize isolation and amplification.

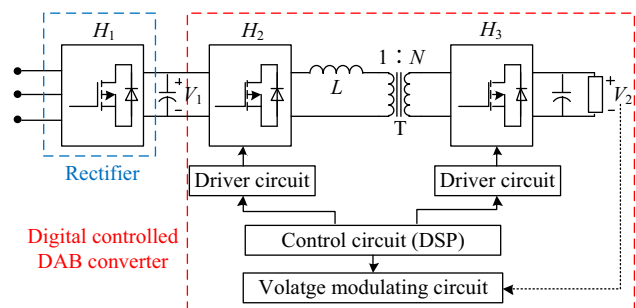
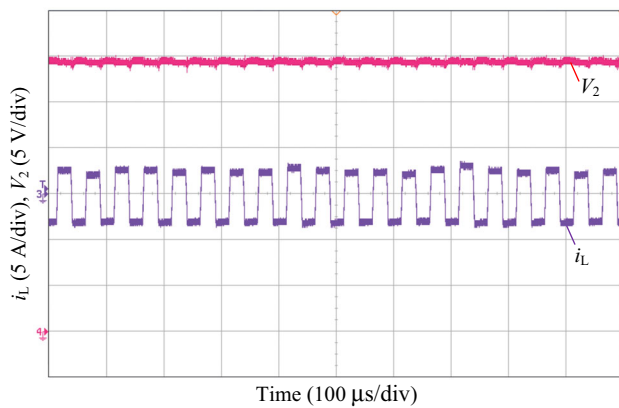
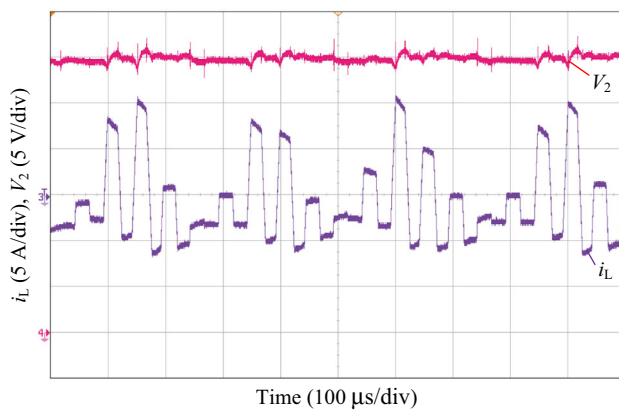
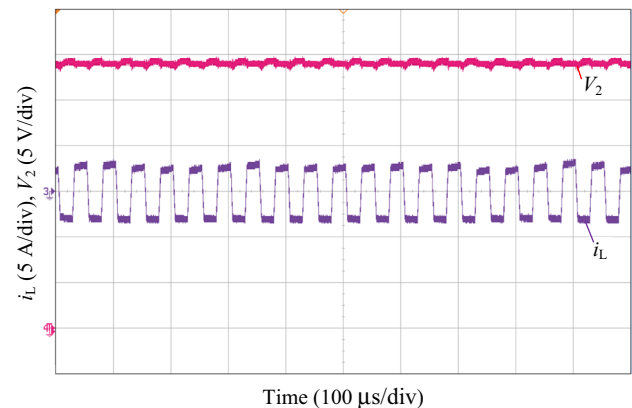
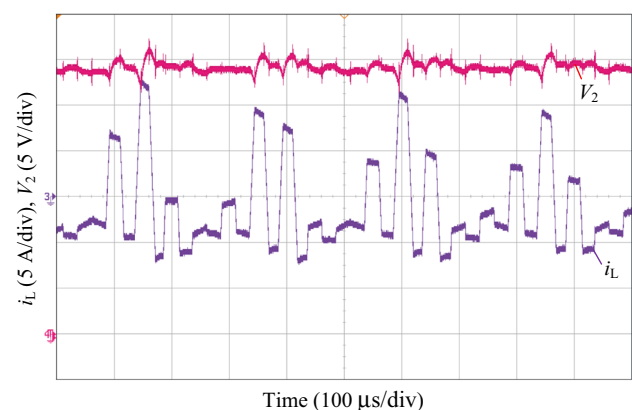


Fig. 7 Functional diagram of experimental platform

(a) Inductor current and output voltage when  $k=0.52$ (b) Inductor current and output voltage when  $k=0.58$ **Fig. 8** Experimental results ( $R_C = 0.45 \Omega$ )

The experimental results with  $R_C = 0.45 \Omega$  are shown in Fig. 8. When  $k = 0.52$ , the system is stable. But when  $k = 0.58$ , low frequency oscillations appears on the waveforms of the output voltage and the inductor current. It can be found from Fig. 8b that the inductor current is asymmetrical about half switching period. This phenomenon can lead to the transformer magnetic bias and even cause the core saturation problem and audible noise. Moreover, the oscillations on the output voltage can also decrease the quality of power supply.

The experimental results with  $R_C = 0.58 \Omega$  are shown in Fig. 9. When  $k = 0.38$ , the system is stable. But when  $k = 0.48$ , low frequency oscillations appears on the waveforms of the output voltage and the inductor current. Comparing between Figs. 8 and 9, the experimental results validate that  $R_C$  has greater influences on the system as the stability boundary is decreased significantly when  $R_C$  is increased. Because of the existence of some practical limitations, such as various parasitic parameters, device model imperfections and dead effect and, there are some differences on amplitude between experimental and simulation waveforms. Furthermore, there are small deviations of  $k$  between experimental results and theoretical calculation.

(a) Inductor current and output voltage when  $k=0.38$ (b) Inductor current and output voltage when  $k=0.48$ **Fig. 9** Experimental results ( $R_C = 0.58 \Omega$ )

## 5 Conclusion

In this paper, the dynamics and stability of a digitally controlled DAB converter have been analyzed. This paper presents a full discrete-time modeling method for the digitally controlled DAB converter with output voltage closed loop. The output capacitor ESR and one step delay in the digital controller are taken into account in the full discrete-time model. Based on this model, the stabilities of the DAB converter versus the proportional controller parameter and the output capacitor ESR are analyzed and then the critical values and the bifurcation types are accurately predicted. Further, this paper also finds that the stability region of the proportional controller parameter is expanded significantly when capacitor ESR  $R_C$  is decreased. So when designing a DAB converter in practice, it is quite important and necessary to take  $R_C$  into account. The analysis in this paper provides useful guidelines for the appropriate design and control of the converter, thereby keeping the bifurcations far enough from the normal operating conditions in parameter space.

**Acknowledgements** This work was supported by National Natural Science Foundation of China (NSFC) (No. 51207126).



**Open Access** This article is distributed under the terms of the Creative Commons Attribution 4.0 International License (<http://creativecommons.org/licenses/by/4.0/>), which permits unrestricted use, distribution, and reproduction in any medium, provided you give appropriate credit to the original author(s) and the source, provide a link to the Creative Commons license, and indicate if changes were made.

## References

- [1] Li WH, Xu C, Yu HB et al (2015) Energy management with dual droop plus frequency dividing coordinated control strategy for electric vehicle applications. *J Mod Power Syst Clean Energy* 3(2):212–220. doi:10.1007/s40565-015-0123-1
- [2] Inoue S, Akagi H (2007) A bidirectional DC-DC converter for an energy storage system with galvanic isolation. *IEEE Trans Power Electron* 22(6):2299–2306
- [3] Cho YW, Cha WJ, Kwon JM et al (2016) High-efficiency bidirectional DAB inverter using a novel hybrid modulation for stand-alone power generating system with low input voltage. *IEEE Trans Power Electron* 31(6):4138–4147
- [4] Naayagi RT, Forsyth AJ, Shuttleworth R (2012) High-power bidirectional DC-DC converter for aerospace applications. *IEEE Trans Power Electron* 27(11):4366–4379
- [5] Engel SP, Stieneker M, Soltan N et al (2015) Comparison of the modular multilevel DC converter and the dual-active bridge converter for power conversion in HVDC and MVDC grids. *IEEE Trans Power Electron* 30(1):124–137
- [6] Zhao B, Song Q, Liu WH et al (2014) Overview of dual-active-bridge isolated bidirectional DC-DC converter for high-frequency-link power-conversion system. *IEEE Trans Power Electron* 29(8):4091–4106
- [7] Zhang K, Shan Z, Jatskevich J (2017) Large- and small-signal average value modeling of dual-active-bridge DC-DC converter considering power losses. *IEEE Trans Power Electron* 32(3):1964–1974
- [8] Dutta S, Hazra S, Bhattacharya S (2016) A digital predictive current-mode controller for a single-phase high-frequency transformer-isolated dual-active bridge DC-to-DC converter. *IEEE Trans Ind Electron* 63(9):5943–5952
- [9] Hou N, Song W, Wu M (2016) Minimum-current-stress scheme of dual active bridge DC-DC converter with unified-phase-shift control. *IEEE Trans Power Electron* 31(12):8552–8561
- [10] Huang J, Wang Y, Li Z et al (2016) Unified triple-phase-shift control to minimize current stress and achieve full soft-switching of isolated bidirectional DC/DC converter. *IEEE Trans Ind Electron* 63(7):4169–4179
- [11] Rodriguez A, Vazquez A, Lamar DG et al (2014) Different purpose design strategies and techniques to improve the performance of a dual active bridge with phase-shift control. *IEEE Trans Power Electron* 30(2):790–804
- [12] Li ZQ, Wang Y, Shi L et al (2016) Optimized modulation strategy for three-phase dual-active-bridge DC-DC converters to minimize RMS inductor current in the whole load range. In: 2016 IEEE 8th international power electronics and motion control conference (IPEMC-ECCE Asia), Hefei, China, 22–26 May 2016, pp 2787–2791
- [13] Maksimovic D, Zane R, Erickson R (2004) Impact of digital control in power electronics. In: Proceeding of the 16th international symposium on power semiconductor devices and ICs (ISPSD '04), Kitakyushu, Japan, 24–27 May 2004, pp 13–22
- [14] Deane JHB, Hamill DC (1990) Instability, subharmonics, and chaos in power electronic systems. *IEEE Trans Power Electron* 5(3):260–268
- [15] Hamill DC, Deane JHB, Jefferies DJ (1992) Modeling of chaotic DC-DC converters by iterated nonlinear mappings. *IEEE Trans Power Electron* 7(1):25–36
- [16] Deivasundari P, Uma G, Ashita S (2013) Chaotic dynamics of a zero average dynamics controlled DC-DC Cuk converter. *IET Power Electron* 7(2):289–298
- [17] Verghese GC, Elbuluk ME, Kassakian JG (1986) A general approach to sampled-data modeling for power electronic circuits. *IEEE Trans Power Electron* PE-1(2):76–89
- [18] Tse CK, Di BM (2002) Complex behavior in switching power converters. *Proc IEEE* 90(5):768–781
- [19] Zhao C, Round SD, Kolar JW (2010) Full-order averaging modelling of zero-voltage-switching phase-shift bidirectional DC-DC converters. *IET Power Electron* 3(3):400–410
- [20] Costinett D (2015) Reduced order discrete time modeling of ZVS transition dynamics in the dual active bridge converter. In: 30th Annual IEEE applied power electronics conference and exposition (APEC), Charlotte, NC, USA, 15–19 March 2015, pp 365–370
- [21] Costinett D, Zane R, Maksimovic D (2014) Discrete time modeling of output disturbances in the dual active bridge converter. In: 29th Annual IEEE applied power electronics conference and exposition (APEC), Fort Worth, TX, USA, 16–20 March 2014, pp 1171–1177
- [22] Costinett D, Zane R, Maksimovic D (2012) Discrete-time small-signal modeling of a 1 MHz efficiency-optimized dual active bridge converter with varying load. In: 13th IEEE workshop on control and modeling for power electronics (COMPEL), Kyoto, Japan, 10–13 June 2012, pp 1–7
- [23] Inoue S, Akagi H (2006) A bidirectional isolated DC-DC converter as a core circuit of the next-generation medium-voltage power conversion system. *IEEE Trans Power Electron* 22(2):535–542
- [24] De Doncker RWAA, Divan DM, Kheraluwala MH (1991) A three-phase soft-switched high-power-density DC/DC converter for high-power applications. *IEEE Trans Ind Appl* 27(1):796–805

**Ling SHI** received the B.S. degree in electrical engineering from Xidian University, Xi'an, China, in 2014. She is currently working toward the M.S. degree at Department of Electrical Engineering, Xi'an Jiaotong University, Xi'an, China. Her research interests include the modeling and stability analysis of the dual active bridge converters.

**Wanjun LEI** received the B.S., M.S., and Ph.D. degrees in electrical engineering from Xi'an Jiaotong University, Xi'an, China, in 2000, 2004, and 2008, respectively. He is an Assistant Professor with the Department of Industry Automation, Power Electronics, and Renewable Energy Research Center, Xi'an Jiaotong University, and also with the State Key Laboratory of Electrical Insulation and Power Equipment, School of Electrical Engineering, Xi'an Jiaotong University. He is a Member of the China Power Supply Society. His research interests include power electronics inverter, active power filter, reactive power compensation, power quality control technique, etc.

**Zhuoqiang LI** received the B.S. degree in Electrical Engineering from Xi'an Jiaotong University, Xi'an, China, in 2014. He is currently working toward the M.S. degree at Department of Electrical Engineering, Xi'an Jiaotong University, Xi'an, China. His research interests include bidirectional dc-dc converters.

**Yao CUI** received the B.S. degree in Electrical Engineering from Henan University of Science and Technology, LuoYang, China, in 2013. He is currently working toward the M.S. degree at Department of Electrical Engineering, Xi'an Jiaotong University, Xi'an, China.



His research interests include control techniques for paralleled converters.

**Jun HUANG** received the B.S. degree in electrical engineering from Xi'an Jiaotong University, Xi'an, China, in 2009, where he is currently working toward the Ph.D. degree in the State Key Laboratory of Electrical Insulation and Power Equipment, School of Electrical Engineering. His research interests include high-frequency-link power conversion system, isolated bidirectional dc-dc converters, and high-power IGBT drivers.

**Yue WANG** received the B.S. and Ph.D. degrees from Xi'an Jiaotong University, Xi'an, China, in 1994 and 2004, respectively, and the M.S. degree from Beijing Jiaotong University, Beijing, China, in 2000. He is currently a Professor at Xi'an Jiaotong University. His current research interests include active power filters, wind power generation, motor drives, multilevel converters, and VSC-HVdc. He is currently with the State Key Laboratory of Electrical Insulation and Power Equipment, School of Electrical Engineering, Xi'an Jiaotong University.

